https://dx.doi.org/10.1016/j.jclepro.2023.139857

Effects of Residual Water on Mechanical Properties of Cold Mix Based Semi-Flexible Pavement Composite Towards a Sustainable Paving Material

Xing Cai
Post-Doctoral Research Fellow
The Hong Kong Polytechnic University
Hung Hom, Kowloon, Hong Kong
Email: tsing2017@foxmail.com

Prabin Kumar Ashish
Assistant Professor
Department of Civil Engineering
Indian Institute of Technology Kanpur
Kanpur, India
Email: pkashish@iitk.ac.in

Zhen Leng ***(Corresponding Author)***
Professor
Department of Civil and Environmental Engineering
The Hong Kong Polytechnic University
Hung Hom, Kowloon, Hong Kong
Email: zhen.leng@polyu.edu.hk

Zhifei Tan
Post-Doctoral Research Fellow
Department of Civil and Environmental Engineering
The Hong Kong Polytechnic University
Hung Hom, Kowloon, Hong Kong
Email: zhi-fei.tan@connect.polyu.hk

Hainian Wang
Professor
Key Laboratory for Special Area Highway Engineering of Ministry of Education
Chang'an University
Xi'an, China
Email: wanghn@chd.edu.cn

Word Count: 6,463 words + 4 table (250 words per table) = 7,463 words

ABSTRACT

This study is an attempt to replace Hot Mix Asphalt (HMA) with Cold Mix Asphalt (CMA) to prepare Porous Asphalt (PA) skeleton for improving the sustainability of Semi-Flexible Pavement (SFP) composite material. Since CMA contains asphalt emulsion, the interaction between emulsion and cement-based grouting material is expected to affect the mechanical properties of the final SFP composite. Therefore, this study investigates the effects of water remaining in the PA mixture at the time of grouting on the mechanical properties of CMA based SFP composite (C-SFPM), using HMA based SFP composite (H-SFPM) as a reference. To prepare C-SFPM, emulsified PA specimens were grouted after different amounts of water (10%, 30%, 60% and 90% by weight, respectively) evaporated from the compacted specimen. The strength, stiffness, moisture damage resistance, ravelling resistance, interfacial bond strength, and microstructural change in C-SFPM and H-SFPM were evaluated at different curing periods. Different mechanical parameters were found to be significantly affected by the time of grouting. Specifically, the detrimental effect of water present in the emulsified PA was identified from ravelling based laboratory evaluation (Cantabro loss value as high as 97.9% was observed). The microstructural analysis also indicated that the formation of hydration product in C-SFPM would be significantly influenced by the amount of water present in the emulsified PA mixture at the time of grouting. Overall, this study indicates that water present in the emulsified mixture has a negative effect on the mechanical properties of C-SFPM.

Keywords: Semi-Flexible Pavement, Cold Mix Asphalt, Water Evaporation, Hot Mix Asphalt, Strength, Stiffness.

1. INTRODUCTION

Permanent deformation, moisture damage, and cracking under different vehicular and environmental loadings, are some of the major concerns of asphalt pavement. Similarly, poor riding quality, high tyre-road noise, heat generation due to friction, etc., are the major concerns of cement concrete pavement. Interestingly, the primary concerns with asphalt pavement are almost absent in cement concrete pavement and vice-versa. Therefore, an attempt was made in the past to develop a composite pavement material which can assimilate the advantages of asphalt and cement concrete pavements. As a result, Semi-Flexible Pavement (SFP) composite material was developed, which primarily consists of Porous Asphalt (PA) skeleton filled with cement-based grouting material. The PA skeleton provides flexibility, whereas the cement-based grout provides rigidity to the SFP composite. About 65% to 75% of the total SFP volume is comprised of asphalt mixture, while the remaining 25% to 35% of the volume is filled with cement-based grouting material.

It is worth noting that the majority of the referred literature on SFP composite has utilized Hot Mix Asphalt (HMA) based PA skeleton for subsequent grouting *(1-7)*. It is a well-established fact that higher degree of greenhouse gas emission and health-related concerns for the on-site team are some of the major concerns of HMA based technologies *(8-11)*. As a result, the sustainability quotient of HMA based SFP technology is substantially low. Attempts have been made in the recent past to develop technologies such as Cold Mix Asphalt (CMA) to improve the sustainability quotient by a substantial extant *(12-15)*. In fact, the thrust on sustainable construction practices (including the roadway sector) is more than ever to achieve the carbon neutrality goal set by different countries *(16)*. Therefore, considering the lower degree of sustainability quotient associated with HMA based SFP composite material (H-SFPM), an attempt was made in this study to utilize CMA to improve its sustainability quotient.

It is known that a substantial part of the emulsion in CMA mixture is water (about 35%-50% by the total weight of the emulsion). The water evaporates with time, which helps improve the strength of conventional CMA mixture after demulsification *(17-21)*. Similarly, the strength of cement-based grouting material increases after hydration. As far as the interaction between emulsion and cement-based grout is concerned, it is supposed that a stronger interlaced interface may form since the hydration products can penetrate into the emulsion during their curing period. Du et al. *(22)* reported that emulsion in cement-based grouting material helps in reducing the negative effect of drying shrinkage on mechanistic properties (such as strength, stiffness, cracking resistance) due to the formation of emulsion residue film over cement paste. However, on the other hand, the presence of emulsion decelerates the cement hydration process *(23-25)*. The above information clearly indicates that consideration should be given to the water present in the emulsified mixture at the time of grouting for the development of CMA based SFP composite material (C-SFPM). In this context, tentative research is conducted to investigate on whether there is an optimal grouting time for the design of C-SFPM with improved properties.

Therefore, this study aims to understand the effects of grouting time on the mechanical properties of C-SFPM. Change in the mechanistic parameters has also been compared with the corresponding parameters of H-SFPM. It is an innovative attempt to replace HMA mixture in SFP with CMA mixture. The optimal grouting time for C-SFPM is an interesting topic worthy of further study. It is expected that the findings from this study would play a critical role in understanding the feasibility of CMA for improving the sustainability quotient associated with existing SFP technology.

2. MATERIALS

Fig.1 shows the selected aggregate gradation. Lime was utilized as filler for the preparation of PA skeleton (3% by the total weight of aggregate). The basic properties of the materials, including the emulsion and asphalt binder utilized for the preparation of PA, the cement grout and superplasticizer are presented in Table 1. Specifically, a cationic and medium-setting asphalt emulsion was used in this research.

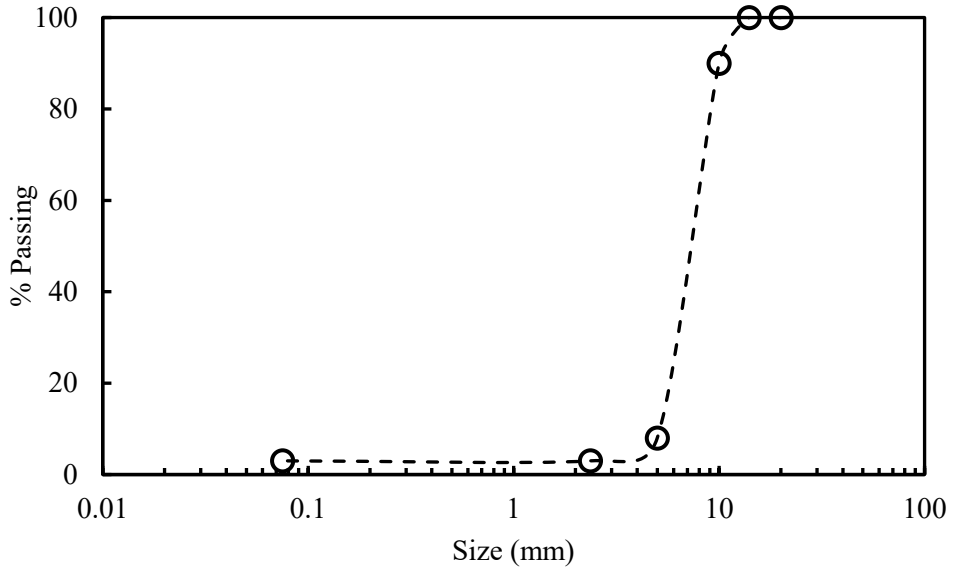

Fig.1: Aggregate gradation

Table 1: Basic properties of materials

Properties of emulsion residue					
Residue content (%)	Penetration (25 ℃, 0.1 mm)	Softening point (℃)	Ductility (5 ℃, cm)	Storage stability	
				1 day (%)	5 day (%)
62.4	64	50	67.2	0.3	2.1

Basic properties of asphalt binder		
Penetration (25 ℃, 0.1 mm)	Softening point (℃)	Viscosity (135 ℃, mPa·s)

64.5			48.5		477.5	
Chemical composition of cement						
SiO_2	Fe_2O_3	Al_2O_3	CaO	MgO	SO_3	Other
20.5%	3.3%	6.6%	66.4%	0.7%	2.73%	<1%
Basic properties of superplasticizer						
Colour		Specific gravity		Alkali content		Chloride content
Yellow		1.04-1.08		0.7%		<0.01%
Physical properties of aggregates						
		Bulk specific gravity (g/cm^3)		Apparent specific gravity (g/cm^3)		Moisture content (%)
Course aggregate (5–14 mm)		2.581		2.598		0.13
Fine aggregate (0.075–5 mm)		2.577		2.601		0.13
Mineral filler		/		2.631		0.85

3. EXPERIMENTAL PROGRAM

Upon the basic characterization of different materials, the next task was to determine the optimal emulsion (for C-SFPM) and asphalt binder (for H-SFPM) content. The optimal number of Marshall blows for achieving the target air void (30%) in the PA skeleton was subsequently ascertained. The appropriate composition for grouting materials based on strength and flow properties was further identified. Different grouting times were chosen for C-SFPM. Mechanistic characterization at different curing periods were conducted, as well as interface characterization, as briefly described in the subsequent section. Fig.2 shows the flow chart for different tasks undertaken in this study.

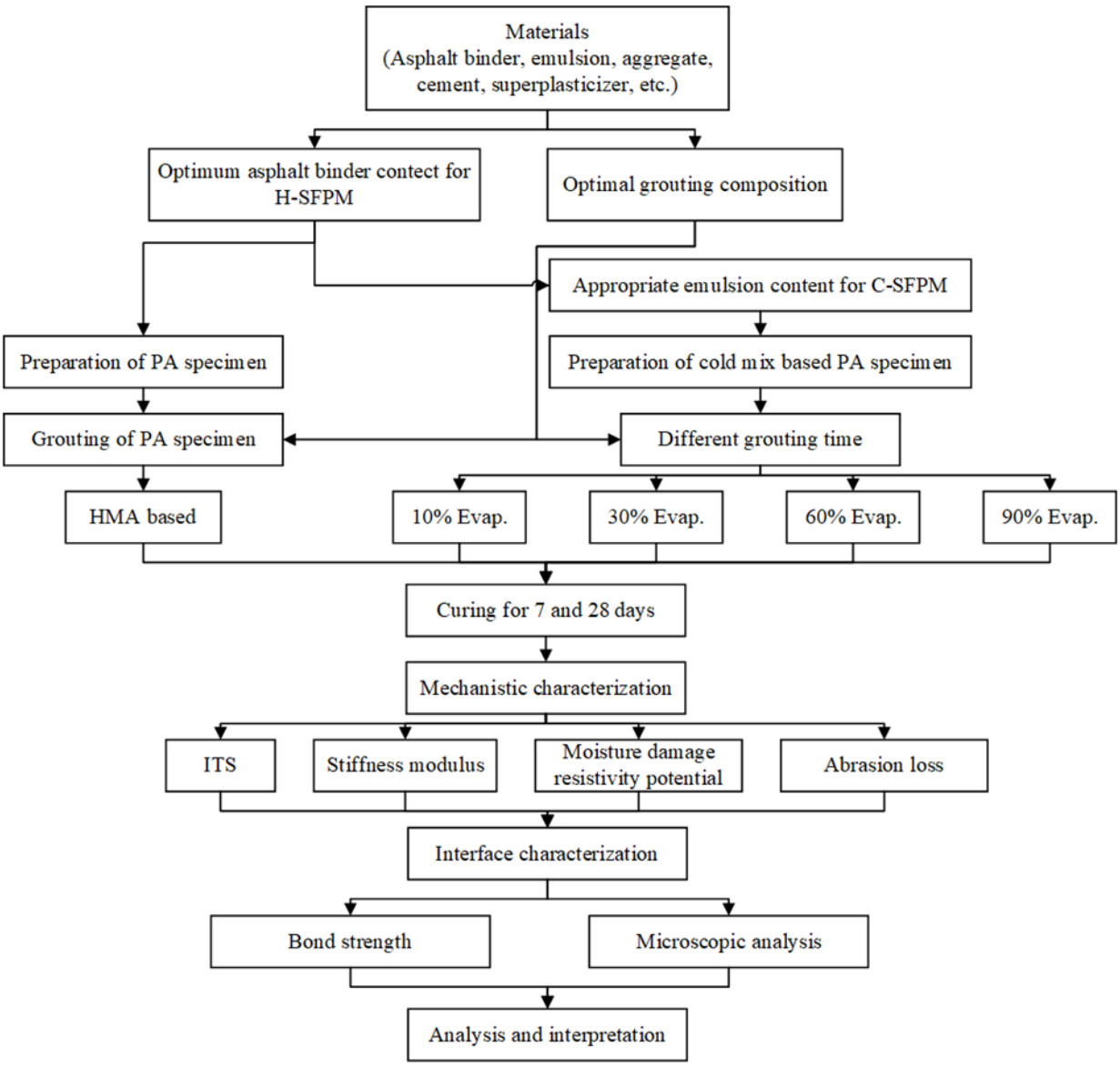

Fig.2: Overall experimental program

4. PREPARATION OF HMA AND CMA BASED PA SKELETON

4.1 Optimal asphalt binder and emulsion content

The optimal asphalt binder content for H-SFPM was ascertained based on the drain-down criteria, as suggested by other researchers *(26-29)*. As per the specification for open-graded asphalt mixture, the permissible limit for drain-down is 0.3% (by the weight of the asphalt mixture). Therefore, the drain-down value for loose asphalt mixtures prepared at different binder content was initially measured as per ASTM D7064. Fig.3 shows the variation of drain-down value obtained at different binder content. Accordingly, the permissible binder content from drain-down perspective was found to be 3.3% by the weight of the asphalt mixture.

It is important to note that no specific standard is available for preparing emulsified

PA with significantly higher air void (25%-35%). Therefore, for the preparation of emulsified PA in the present study, the emulsion content was chosen in such a way that its residue content is equal to the asphalt binder content in the HMA based PA skeleton. This approach also helped in making a relative comparison between mechanistic parameters evaluated for CMA and HMA based SFP composite mixture at a later stage. Since the asphalt residue content in emulsion utilized in this study was 62.4%, the selected emulsion content was 5.3% by the weight of the emulsified PA mixture.

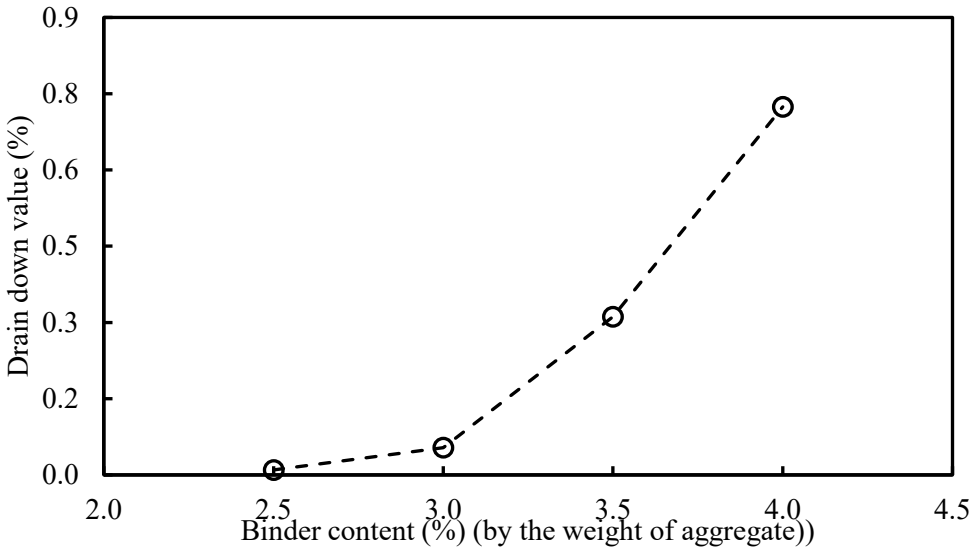

Fig.3: Variation of drain-down value with binder content

4.2 Optimal number of Marshall blows

Unlike conventional dense-graded asphalt mixture, there is no specific recommendation for selecting the appropriate number of Marshall blows to prepare the PA skeleton for the SFP based composite. Some researchers utilized a gyratory compactor *(30-31)*, while others utilized Marshall compactor on one or both faces to achieve the target air-void level in the cylindrical specimens *(32-35)*. In this study, the Marshall compactor with compaction on only one face of the specimen was utilized for sample preparation. Specimens containing optimal asphalt binder content were compacted with varying Marshall blows, and the corresponding air-void was measured as per ASTM D3203. Fig.4 shows the variation of air void with the change in Marshall blows for PA specimens. The variation in air-void of CMA based PA specimens with Marshall blows is similar as that of HMA based ones. The optimal number of Marshall blows was found to be 50, corresponding to the target air void of 30% for PA skeleton. The final air void for emulsified mixture was found to be 30.7%, which is about 0.7% higher than its HMA counterpart.

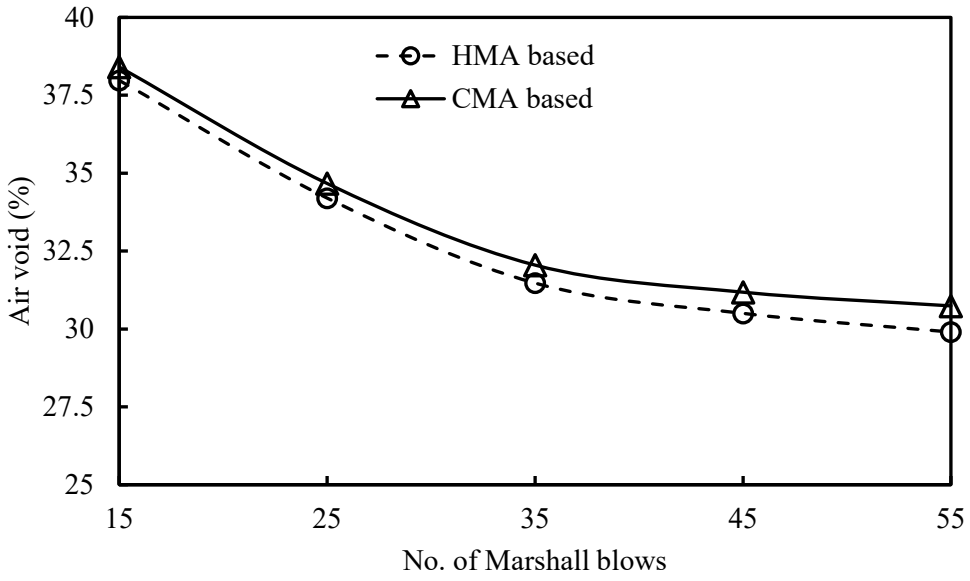

Fig.4: Change in air-void with the change in Marshall blows for HMA and CMA based PA skeleton

4.3 Grout formulation

Cement-based slurry was utilized as grouting material in this study *(37-40)*. Several trials were carried out in the laboratory to get the final grout composition. The mixing of different constituents was carried out using a portable mixer per the general procedure recommended by Oliveira *(1)*. It is important to note that the final grout composition should not only fill the connected voids in the PA skeleton but should also provide sufficient strength to the final SFP composite. Therefore, the flowability, strength and shrinkage-based properties were finally evaluated to select the appropriate grout composition. Table 2 summarizes the flow, strength and shrinkage properties of the final grout. The flow time, strength, as well as shrinkage properties of the final grout composition can be found to be falling well within the acceptable range.

Table 2: Properties of final grout composition

Property	Value*	Requirements
Flow time (sec.)	15.45 (0.15)	12-16 as per Oliveira (2006)
1-day Compressive strength (MPa)	26.14 (3.27)	≥10 MPa as per JTG E30 T0506
7-day Compressive strength (MPa)	55.11 (4.25)	≥20 MPa as per JTG E30 T0506
7-day drying shrinkage value	0.095 (0.009)	≤0.3 as per JTG E30 T0511

** Number outside the bracket is average, while inside is the std. dev. value.*

4.4 Grouting for SFP composite

For H-SFPM, grouting was done after PA skeletons were cooled down to room temperature. For C-SFPM, the evaporation of water from the prepared emulsified mixture was monitored. The corresponding emulsified PA was grouted as soon as it achieved a certain evaporation level. In this research, four evaporation levels (10%, 30%, 60%, and 90%) were selected. Sample Identification Code (ID) and the corresponding state it represents are provided in Table 3. For instance, 10% Evap represents the state where 10% by weight of water has been evaporated in the emulsified mixture at the time of grouting. A special split cylindrical mould was fabricated and used for easy demoulding. The grouting operation was subsequently completed with the help of a table vibrator. At the end of the grouting operation, the extra grout at the top of the grouted specimen was removed. Based on the air void in the PA skeleton and the quantity of the penetrating grout, residual air void in the grouted SFP composite was determined by Eq.1. Table 4 provides the information on the residual air-void for different specimens.

$$Residual\ air\ void\ (\%) = \frac{A \times V - \left(\frac{m_g - m_a}{\rho_g}\right)}{V} \times 100 \quad (1)$$

where A is the air void in the specimen, V is the volume of specimen, m_g is the mass of specimen after grouting, m_a is the mass of specimen before grouting, and ρ_g (= 1.917 gm/cc) is the density of grout.

The residual air void in the C-SFPM was found to be relatively higher than the corresponding H-SFPM (Table 4). Moreover, the average residual air void in the C-SFPM decreased with the increase in water evaporation level from the emulsified PA mixture at the time of grouting. This clearly indicates that the presence of water in the emulsified porous mixture can potentially affect the degree of grouting. Upon grouting, specimens were covered with a plastic sheet and left undisturbed in the split Marshall mould for 24 hours. Subsequently, specimens were demoulded and kept under 90%-95% humidity level for curing (7 days or 28 days).

Table 3: Specimen identification information

Sample ID	Evaporated water in the emulsified mix. at the time of grouting (%)	Remaining water in the emulsified mix. at the time of grouting (%)
10% Evap.	10	90
30% Evap.	30	70
60% Evap.	60	40
90% Evap.	90	10
HMA based	N/A	N/A

Table 4: Residual air voids after grouting[#]

Sample ID	Specimen air void (%)	Density of grout	Residual air void (%)
10% Evap.	30.9 (0.18)	1.917 g/cc	10.45 (0.33)

30% Evap.	31.2 (0.08)	9.90 (0.34)
60% Evap.	31.8 (0.20)	9.03 (0.17)
90% Evap.	32.4 (0.19)	8.40 (0.58)
HMA based	29.8 (0.46)	6.78 (0.88)

[#]*Number outside the bracket is average, while inside is the std. dev. value*

5. MECHANISTIC CHARACTERIZATION

5.1 Indirect Tensile Strength (ITS)

The ITS values of different SFP composites were evaluated on 100 mm dia. specimen using a loading rate of 51 mm/minutes as per ASTM D6931. The specimens were kept in a conditioning chamber at 20 ºC for 4 hours before testing. Four replicate specimens were prepared for evaluating the strength parameter. The maximum load carried by the specimen was recorded to evaluate the indirect tensile strength value as per Eq.2.

$$ITS = \frac{2P}{\pi DT} \quad (2)$$

where ITS = indirect tensile strength (kPa), P = peak load (kN); and D and T = diameter and thickness of the specimen respectively (m).

5.2 Indirect Tensile Stiffness Modulus (ITSM)

The ITSM value was evaluated for two specimens as per BS EN12697-26 specifications at 20ºC. Four replicate specimens were utilized for evaluating the stiffness parameter. The Poisson's ratio for ITSM evaluation (Eq.3) was assumed to be 0.25 as per recommendations made in the referred literature *(2)*. Each specimen was subjected to 40 conditioning cycles before actual measurement with the last 5 load pulses.

$$ITSM = \frac{P\times(\mu+0.27)}{DT} \quad (3)$$

where ITSM = Indirect tensile Stiffness Modulus of the specimen (MPa); P = Peak load to the specimen (N); μ = Poisson's ratio; and D, and T = diameter and thickness of the specimen (mm).

5.3 Moisture damage resistance

ASTM T-283 based freeze-thaw approach was utilized to evaluate the moisture damage resistance. Unlike the standard process for HMA (which requires 70%-80% sample saturation before starting the freeze-thaw process), the specimens were saturated under standard vacuum pressure condition for 30 minutes. This is due to the fact that the majority of the connected pores in the specimen are already filled with cement grout. As a result, the intrusion of water during the saturation process was relatively low. In fact, 30 minutes time period for conditioning has also been recommended by IRC:111*(42)* for SFP based composite specimens. Subsequently, the specimens were kept at -18ºC for 16 hours followed by 24 hours in water at 60ºC. Finally, the specimens were kept under a controlled temperature of 25ºC before conducting the ITS test. Three replicate specimens were utilized for evaluating the strength parameter. The moisture damage resistance was

evaluated using Tensile Strength Ratio (TSR) as per Eq.4.

$$TSR\ (\%) = \frac{ITS_{Conditioned}}{ITS_{Unconditioned}} \times 100 \quad (4)$$

where TSR is tensile strength ratio (%); and $ITS_{Conditioned}$ and $ITS_{Unconditioned}$ are indirect tensile strength values for conditioned and unconditioned specimens, respectively (kPa).

5.4 Resistance against ravelling loss

Resistance against ravelling loss was evaluated with the help of the Cantabro test as per ASTM D7064 to get an overall sense on the bonding between different constituents. For this purpose, the Marshall specimens were allowed to abrade for 300 revolutions in the Los Angeles abrasion machine. Finally, the weight loss at the end was evaluated and reported as Cantabro loss (Eq.5). Three replicate specimens were utilized for evaluating the ravelling loss.

$$Cantabro\ loss\ (\%) = \frac{W_1 - W_2}{W_1} \times 100 \quad (5)$$

where W_1 and W_2 are the weight of the specimen, before and after the test.

5.5 Bond strength test

A pull-out test was conducted as per ASTM D4541 to understand the change in bond strength. In order to conduct this test, granite rock slab with a uniform roughness level having the dimension of 200mm X 200mm X 10mm was prepared. The sides of the aggregate slab were sealed with 4mm thick adhesive tape to avoid the spilling of emulsion/asphalt binder from the boundary during the sample preparation stage (Fig.5a). The aggregate slab was subsequently coated with the required amount of emulsion/asphalt binder to maintain the thickness of 200µm *(34, 42)*, calculated as per Eq.6.

$$W = A \times 0.2 \times \rho \quad (6)$$

where W is the required weight of emulsion or bitumen to get a target thickness of 0.2 mm; A is the coating area on the aggregate slab; and ρ is the density of emulsion or bitumen.

Once the required amount of emulsion is uniformly spread over the aggregate slab, the next step was to wait until the required level of water evaporation is achieved (refer to Table 4 for further details). As soon as the targeted level of evaporation was achieved, the grouting operation was completed with the help of the prefabricated rectangular silicon pad (thickness = 5mm) having 9 circular holes with 20mm diameter (Fig.5b; Fig.5c). The prepared specimens were then covered with plastic sheets for 24 hours before removing the silicon pad and then kept under 90%-95% humidity level for subsequent curing (Fig.5d). For HMA based grouted specimens, the same process was applied upon the attainment of room temperature by the coated asphalt binder film on the aggregate slab.

The pull-out test was finally conducted on the specimens at the end of 28 days curing period. Three replicate specimens were utilized to evaluate the interfacial bond strength. The pull-out stub was initially glued to the top of the grout surface with the help of epoxy-based adhesive at the end of 26 days of curing (Fig.5e). The pull-out test was finally conducted with the help of the PosiTest Adhesion tester as per ASTM D4541 with a manually controlled pulling rate of 0.7 MPa/sec (Fig.5f). The maximum interfacial strength

can be directly obtained from the digital display of the equipment.

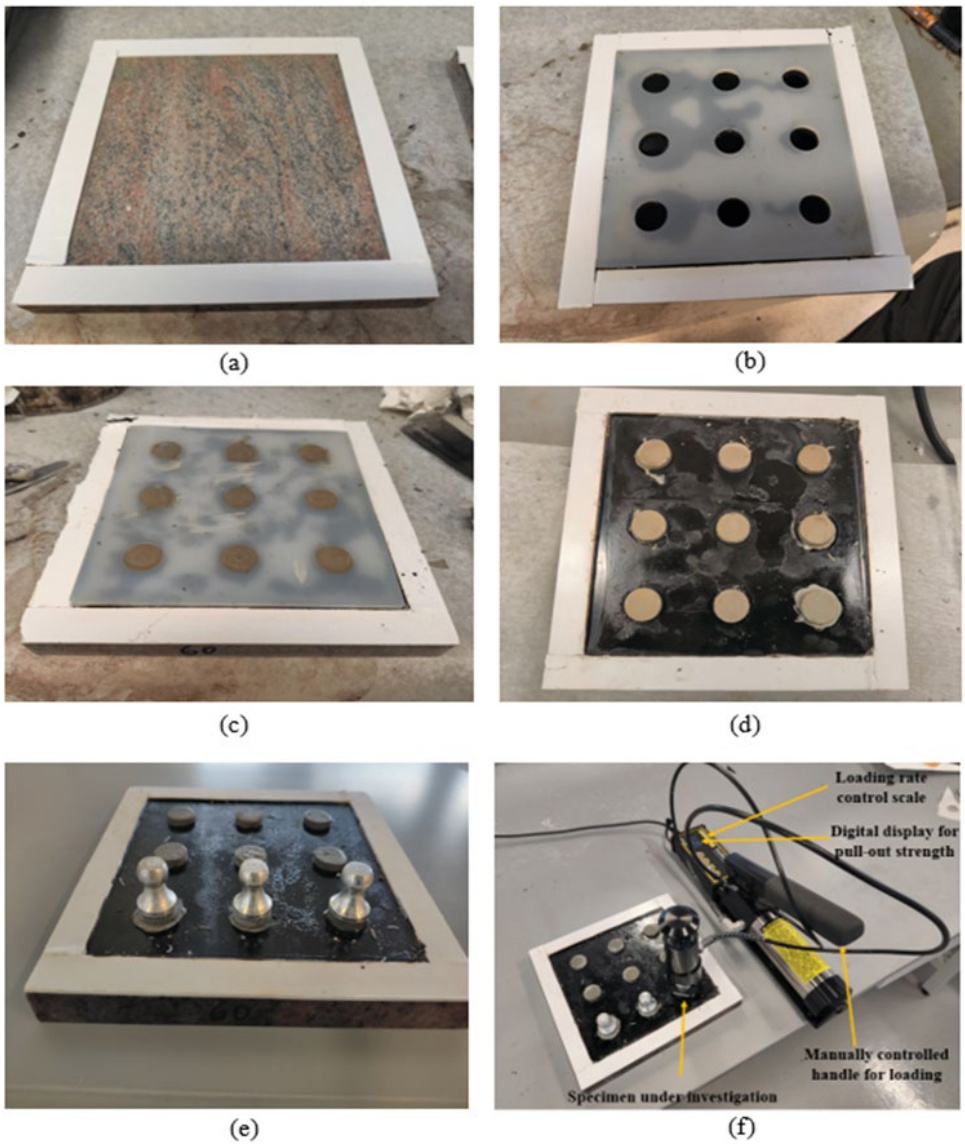

Fig.5: Pull-out test based sample preparation and testing arrangements

5.6 Microscopic analysis

Microscopic analysis of different SFP composite was done with the help of the Scanning Electron Microscope (SEM). SFP based Marshall specimens were prepared as per the procedure explained before (refer to Section 4.4 for more details). Subsequently, upon the completion of a certain curing period (7/28 days), a small specimen required for the SEM test was extracted from the compacted SFP composite. Finally, SEM test was conducted using a tungsten thermionic emission (TESCAN VEGA3) system at an accelerating voltage of 20Kv and a magnification level of 10000x.

6. RESULTS AND DISCUSSION

6.1 Effect of water in the emulsified mix during grouting on SFP strength

Fig.6 shows the variation of ITS value for SFP specimens. The influence of grouting time on the strength parameter is clearly evident from the plot. For example, the 7th day cured ITS value for the specimens grouted after 30%, 60%, and 90% evaporation levels are about 8.6%, 24.1%, and 43.8%, respectively higher compared to the corresponding value after 10% evaporation. Such a response clearly indicates that the larger the amount of water present in the emulsified mixture, the smaller the strength of the final SFP composite. The relatively slower rate of hydration with a proportionally higher amount of water in the emulsified PA skeleton can be considered one of the primary reasons behind such change. In addition, relatively high residual porosity (as shown in Table 4) is also a potential cause. It is also worth noting that despite the similarity in the grade of asphalt binder and emulsion residue for CMA in this research, the strength of H-SFPM is significantly higher than any of the C-SFPM. It is also to be noted that although the strength of the C-SFPM depends on water available in emulsified mixture, the corresponding strength value is still comparable or even higher than a typical dense-graded HMA specimen (0.5-1.3MPa) *(43)*. This signifies that C-SFPM is expected to satisfy the strength requirement even if it is grouted when the water content in the emulsified PA mixture is reasonably high. Finally, non-parametric statistical analysis (using the Tukey's honestly significant difference approach) was carried out to incorporate the variability associated with the strength in the analysis process. Fig. 7 represents the p-value matrix for ITS value obtained for various specimens in this research considering 95% confidence interval. In general, the difference in ITS value between nonadjacent groups was found to be statistically significant, which indicates the negative effect of water present in the emulsified mixture at the time of grouting on the strength of CMA based SFP composite.

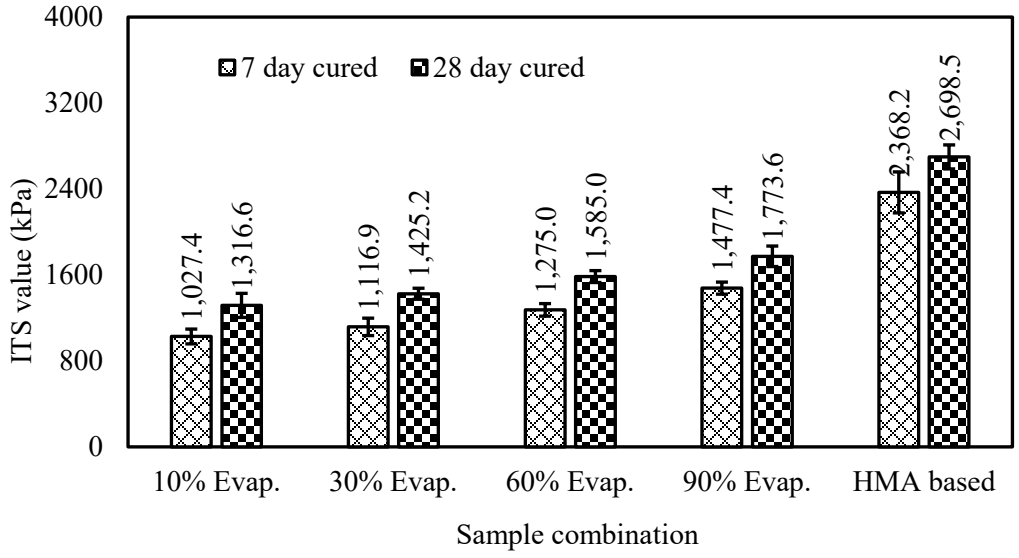

Fig.6: Variation of ITS value with sample grouted at different evaporation level.

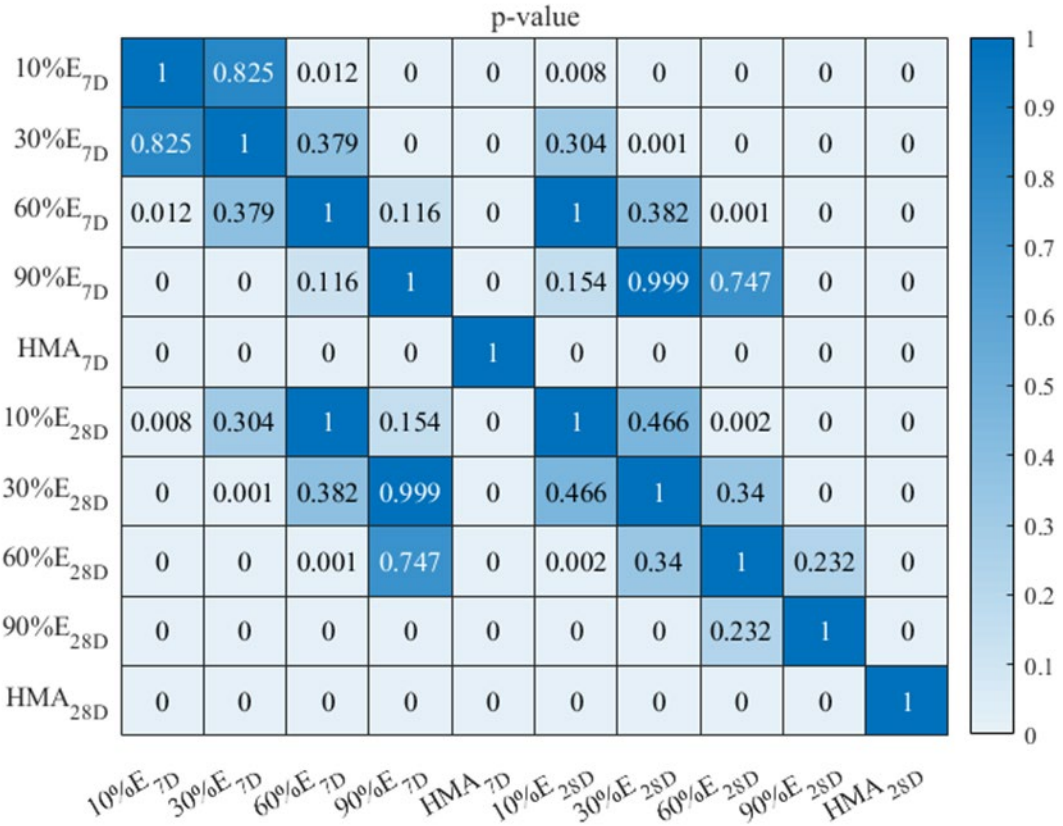

Fig.7: Statistical p-value matrix for ITS value of SFP composite material

6.2 Effect of water in the emulsified mix during grouting on SFP stiffness

Fig.8 shows the variation of ITSM value for the specimens grouted after different evaporation levels from the emulsified mixture. Just like the strength parameter, the influence of grouting time on the stiffness parameter of C-SFPM is evident from the plot. For example, the 7th day cured average ITSM values for specimen grouted after 30%, 60%, and 90% evaporation levels are 294 MPa, 527 MPa, and 1018 MPa, respectively higher than the corresponding values of the grouted specimens after 10% evaporation. As explained in the previous section, a lower rate of hydration and the presence of a proportionally higher amount of water in the emulsified mixture are the primary reasons for such an outcome. Moreover, it is also clear from the plot that the ITSM value of the H-SFPM is significantly higher than the corresponding value of any of the C-SFPM. In addition, the increase in ITSM value for H- SFPM with an increase in curing period from 7 days to 28 days is 2338 MPa, which is relatively higher compared to the corresponding increase for C-SFPM. At the same time, although the ITSM value of C-SFPM is relatively low, the corresponding values are still comparable or even higher compared to a typical dense-graded HMA specimen. Finally, statistical analysis was carried out to incorporate the variability associated with the ITSM value in the analysis process. Fig. 9 represents the p-value matrix for ITSM value obtained for various specimens (considering 95%

confidence interval). It can be inferred from the table that the degree of variability associated with ITSM value is relatively lower compared to the corresponding variability observed for strength evaluation. Overall, the above discussion clearly indicates the negative effect of water present in the emulsified mixture at the time of grouting on the stiffness of C-SFPM.

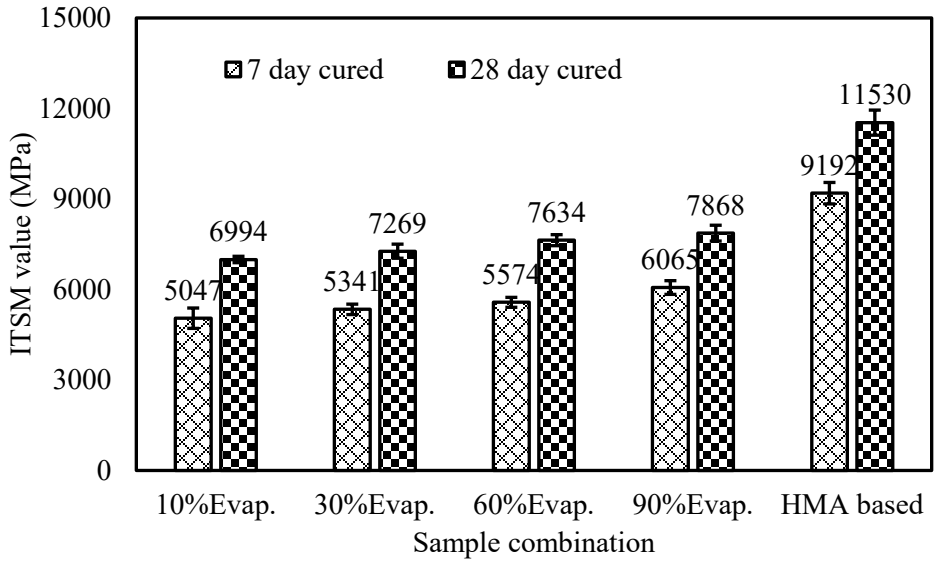

Fig.8: Variation of ITSM value with sample grouted at different evaporation level.

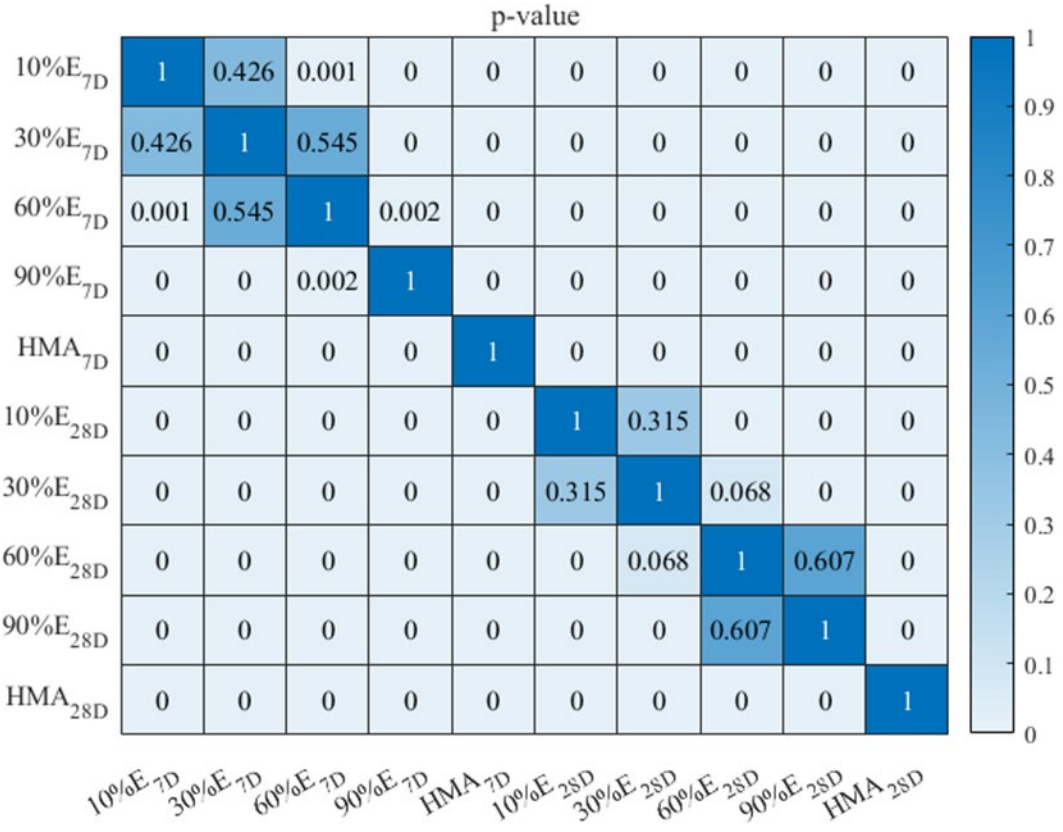

Fig.9: Statistical p-value matrix for ITSM value of SFP composite material

6.3 Effect of water in the emulsified mix during grouting on moisture damage resistance

Fig.10(a, b) shows the variation of TSR value for the specimens grouted at different evaporation levels. Irrespective of the amount of water present in the emulsified mixture, the TSR value was found to be more than 0.8. This indicates that although moisture damage related problem is one of the major concerns with conventional CMA technology, such problem may remain non-existent with C-SFPM. Moreover, a relatively higher TSR value for H-SFPM compared to its CMA counterpart is evident from the plot. Although the information on TSR for C-SFPM is not available in the referred literature, the corresponding values obtained in this research are in line with the reported TSR value for H-SFPM *(26;34-35)*. As far as the influence of the water available in the emulsified mixture is concerned, no specific trend was observed for TSR. Overall, the improvement in the moisture damage resistance of C-SFPM can be explained with the help of three possible phenomena. The first one is related to the protection of aggregate-emulsion residue interface by the grouting material. As a result, the accessibility of water to the aggregate-emulsion residue interface is reduced by a substantial degree. At the same time, the porosity of the SFP composite material reduced due to grouting. Therefore, the possibility of water percolation to such composite material decreased. The third reason is related to the accelerated hydration process of the grouted phase of the SFP composite specimen for 24 hours during the thawing process (at 60ºC). As a result, a relatively higher strength of the conditioned specimen can be expected. Along with the variability associated with TSR based measurement, the third hypothesis could be the possible reason for TSR value of more than 1 for H-SFPM for 7 days cured specimen. In fact, TSR value of more than 1 (1.03 to 1.06) for many of the SFP based composite specimens are also reported by Zachariah et al. *(27)*.

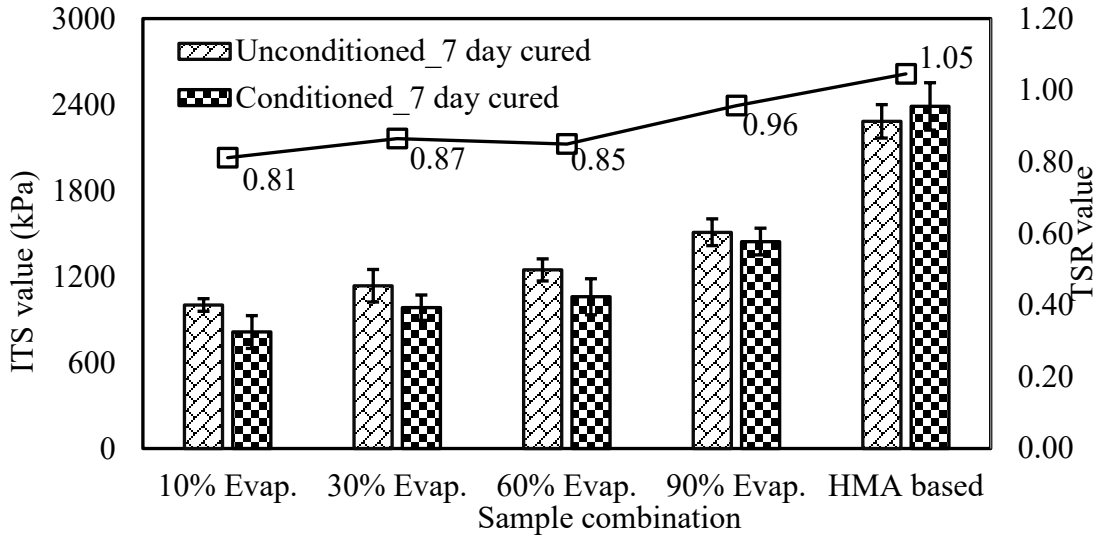

(a)

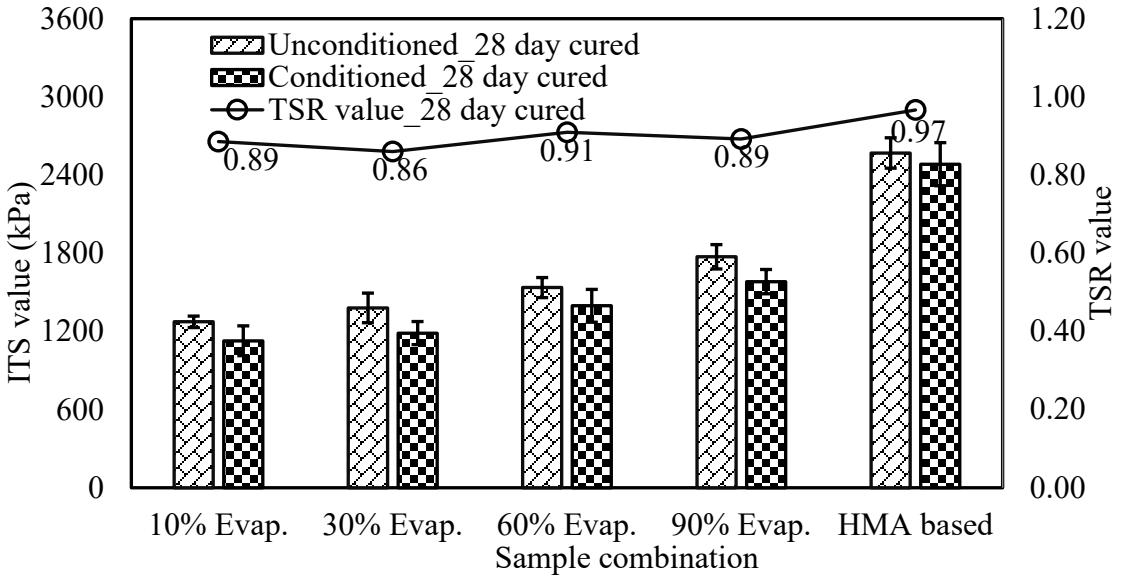

(b)

Fig.10: Variation of TSR value with specimens grouted at different evaporation level and tested after (a) 7 days curing, and (b) 28 days curing.

6.4 Effect of water in emulsified mix during grouting on ravelling resistance

Fig.11 shows the variation of abrasion loss value for the specimens grouted after different evaporation levels from the emulsified mixture. Unlike the strength, stiffness, and moisture damage resistance, where the resulting values for specimen grouted at different evaporation levels were found to be reasonably encouraging, a significantly different inference can be made based on the assessment from abrasion loss test. Cantabro loss value as high as 97.9% was observed for 7 days cured 10% Evap. The acceptable Cantabro loss value for a typical asphalt mixture is around 20%. Only the Cantabro loss value for 28 days cured specimen grouted after 90% water evaporation is marginally higher than the permissible value. Such a response indicates that one should wait for the water to evaporate from the emulsified mixture to a certain extent, or decrease the water cement ratio before grouting.

Moreover, the Cantabro loss value for H-SFPM is within the acceptable range. Statistical analysis was carried out to incorporate the variability associated with the Cantabro loss in the analysis process. Fig. 12 represents the p-value matrix for Cantabro loss obtained for various specimens. Overall, the difference between groups was more significant than the other mechanical parameters. Abrasion loss can be considered among the most important laboratory-based evaluations of C-SFPM.

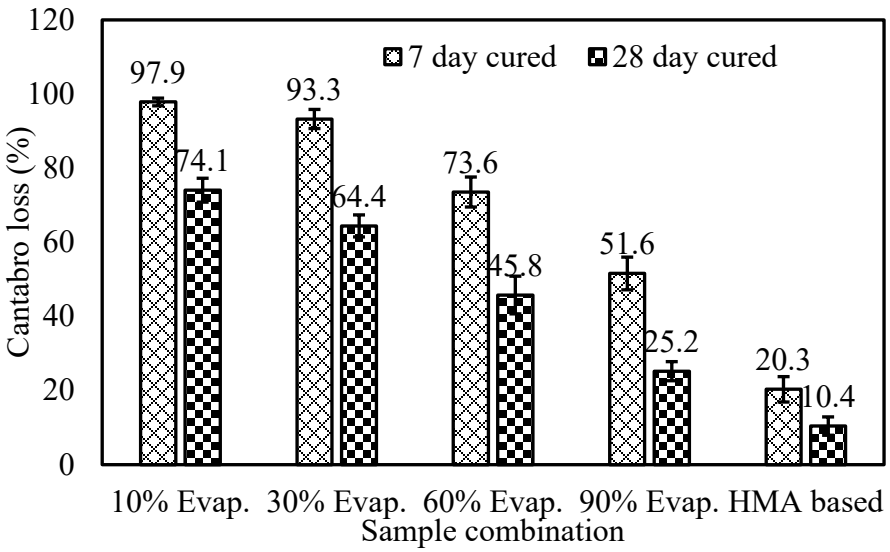

Fig.11: Variation of Cantabro loss value with specimens grouted at different evaporation level and tested after different curing period.

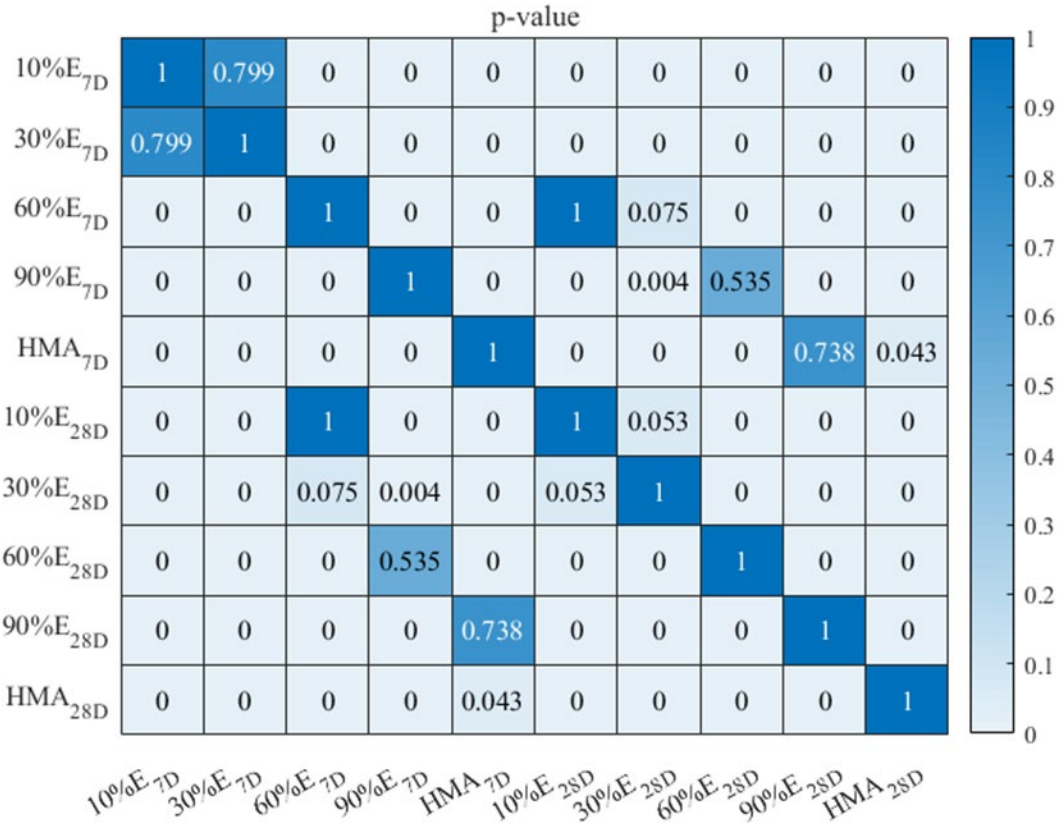

Fig.12: Statistical p-value matrix for Cantabro loss of SFP composite material

6.5 Effect of water in the emulsified mix during grouting on interfacial bond strength

Fig.13 shows the pull-out strength values for the specimens grouted at different evaporation levels after 28 days of curing. It can be observed that as the water evaporation

level increased, the interfacial bond strength also increased. For example, the interfacial bond strength increased from 1.43 MPa to 1.76MPa with an increase in water evaporation level from 10% to 90%. Moreover, the interfacial bond strength with H-SFPM was found to be higher than any of the C-SFPM. Statistical analysis was subsequently carried out considering the variability as highlighted before to understand the variation in a better way. Fig. 14 represents the p-value matrix for pull-out strength obtained for various specimens considering 95% confidence interval. Although the average pull-out strength increased in general, most of the p-values were found to be more than 0.05, indicating an insignificant difference between correspondingly reported values. One of the reasons for such a variability could be the uncontrolled/non-uniform mixing of grout material and emulsion (because emulsion contains water at the time of grouting. Therefore, when the grout material was poured over the emulsion coated aggregate slab, both materials are expected to mix. Consequently, the proportional amount of cement and emulsion residue at the failure interface is expected to vary). In fact, a similarly higher degree of variability for HMA based grouted pull-out strength has also been reported by Zarei et al. *(34)* and Ling et al. *(42)*. The authors believe that further study is needed to decrease such variability.

Along with the pull-out strength value, the failure pattern was also analysed to get an idea about the weakest interface. Fig.15 and Fig.16 show the visuals of the failure interface on the pull-out stub and aggregate slab for the specimens grouted at different evaporation levels, respectively. Failure at the aggregate-emulsion residue interface in most of the cases can be clearly sensed from Fig.15 and Fig.16. Moreover, the aggregate surface at the failure interface is visible for most of the CMA based specimens (Fig.16 a, b, c, d), indicating the adhesive nature of the failure pattern. On the other hand, a thin bitumen layer is still visible at the failure interface for the HMA based specimen (Fig.16e), indicating the cohesive nature of the failure pattern.

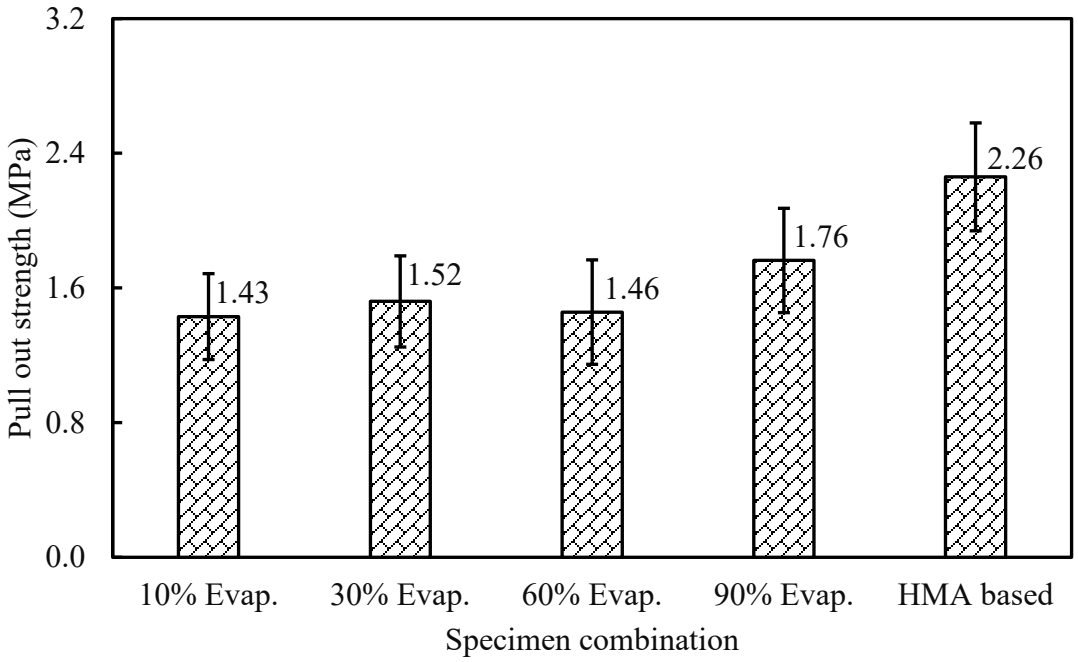

Fig.13: Pull-out strength for specimens grouted at different evap. Level

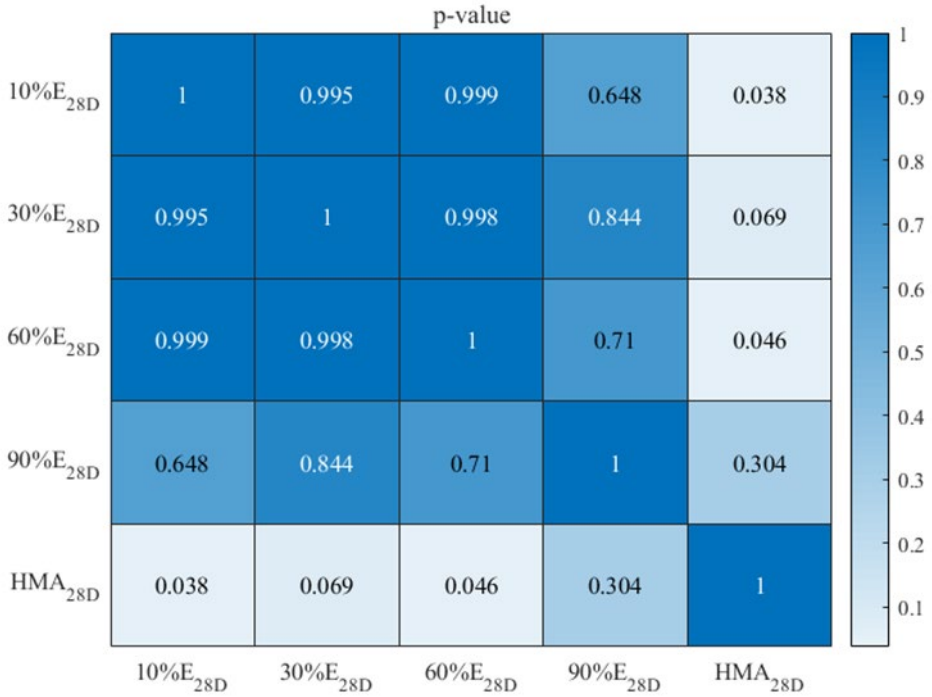

Fig.14: Statistical p-value matrix for pull-out test on SFP based composite specimen

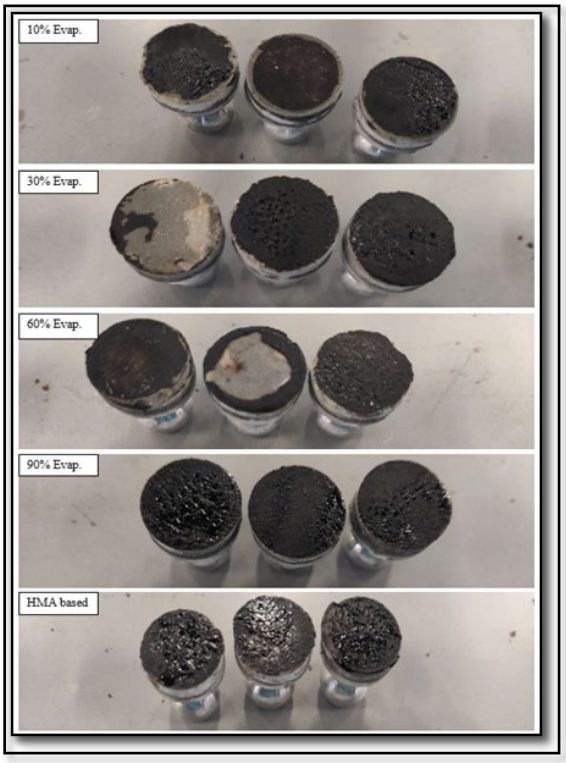

Fig.15: Visuals of failure interface on pull-out stub for specimens grouted at different evap. level

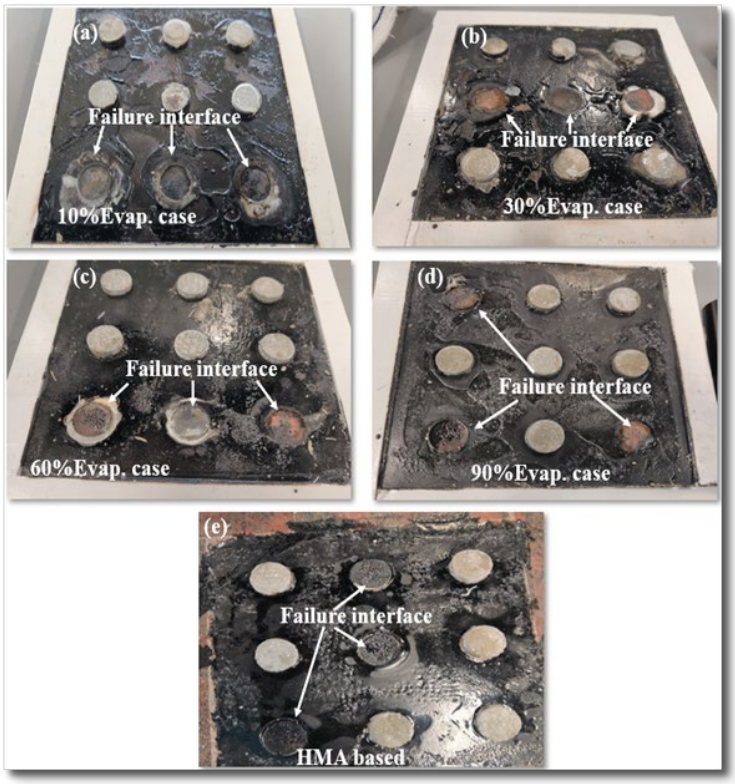

Fig.16: Visuals of failure interface on the aggregate slab for specimens grouted at different evap. level

6.6 Microscopic analysis

Fig.17 and Fig.18 show the SEM images of the samples taken from the interface of the grouted specimens. The formation of major hydration products such as ettringite (calcium sulfoaluminate), CSH (Calcium silicate hydrate), and CH (Calcium hydroxide) is highlighted. One of the important features identified through these SEM images is that a proportional amount of needle-shaped ettringite (formed during the early stage hydration) increased for specimens grouted after a higher amount of water evaporated from the emulsified mixture. In fact, the amounts of ettringite in 10%evap. and 30%evap. are substantially lower compared to those in 60%evap., 90%evap., and HMA based grouted specimens. This demonstrates that the higher the amount of water present in the emulsified mix at the time of grouting, the lower the rate of early-stage hydration. Although ettringite formation is usually related to the setting time, the corresponding hydration product also provides early strength *(44-47)*. As a result, the strength, stiffness and bond strength value of the specimen containing a higher amount of water in the emulsion at the time of grouting was lower. Moreover, while comparing Fig.17 and Fig.18, the proportionally less amount of needle-shaped ettringite is evident for 28 days cured specimens, which can be attributed to the conversion of ettringite to calcium aluminate monosulfate.

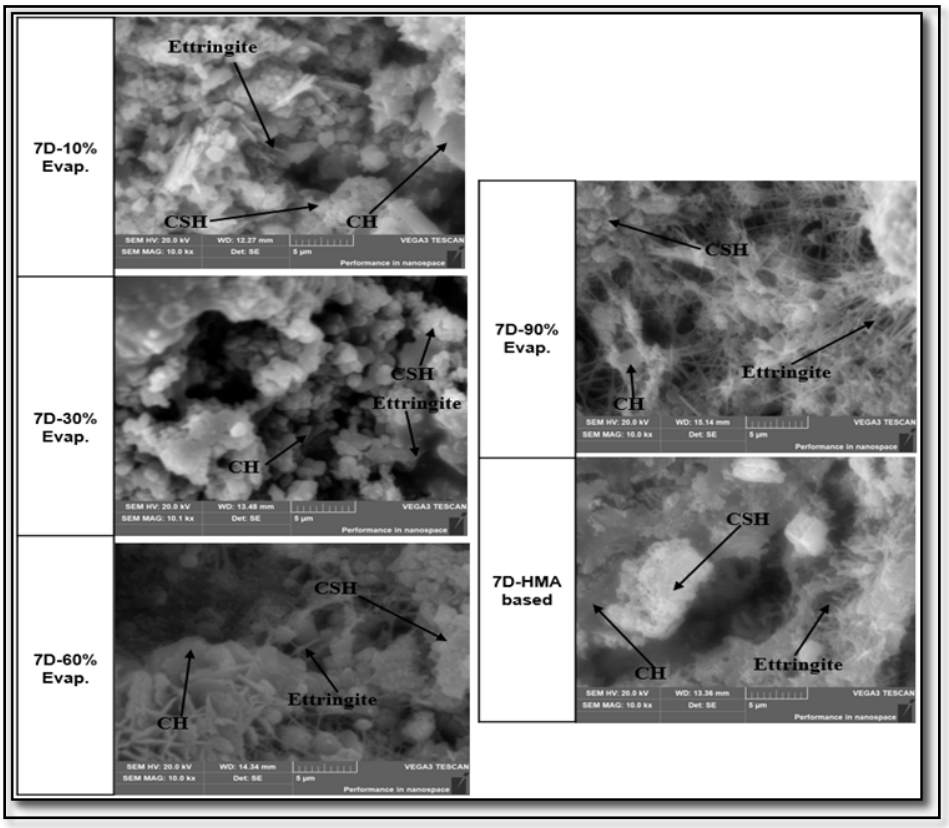

Fig.17: SEM images for from the interface of grouted specimen after 7 days of curing period

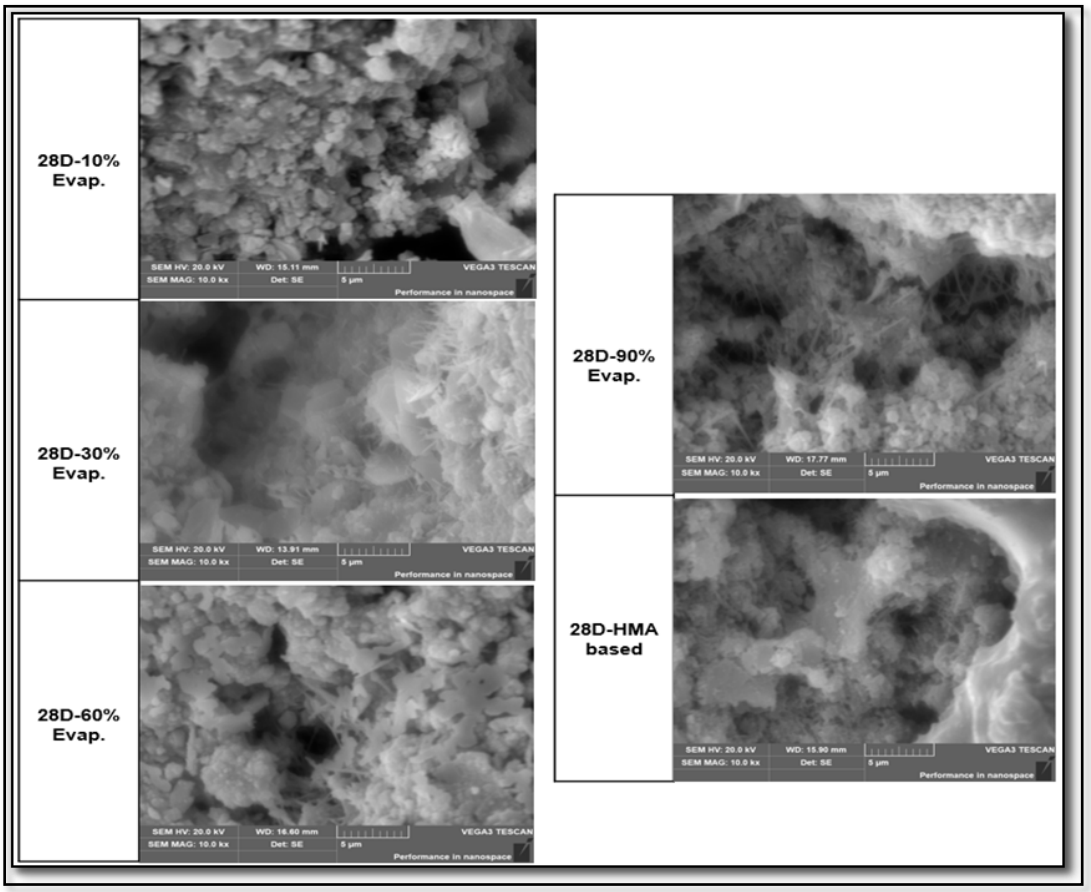

Fig.18: SEM images for samples from the interface of grouted specimen at 28 days curing

7. CONCLUSIONS

This study attempts to understand the role of water present in the emulsified PA mixture at the time of grouting on the mechanistic parameters of C-SFPM. The laboratory test results were also compared with the corresponding parameters of H-SFPM. Grouting to the emulsified PA mixture was done after different degrees of water evaporated from the specimens (10%, 30%, 60% and 90%). The strength, stiffness, moisture damage resistance, ravelling resistance, interfacial bond strength, and microstructural related changes were evaluated in the laboratory. The followings are the major conclusive remarks based on the discussion made in the preceding sections.

- The expected level of strength and stiffness achieved by C-SFPM will be relatively lower if the grouting is conducted when the proportional amount of water present in the emulsified mixture is relatively higher, which is significantly lower than H-SFPM. However, they are all higher than that of the typical dense-graded HMA.
- Although the amount of water present in the emulsified PA mixture at the time of grouting can influence the moisture damage resistance of C-SFPM, the corresponding SFP composite will still be safe from moisture damage even if it is grouted when the amount of water in the emulsified mixture is relatively high.

- Examining ravelling resistance can be among the most important laboratory-based assessment for C-SFPM. As per the experimental results obtained through this research, it is suggested to start the grouting once most of the water is evaporated from the emulsified mixture or reduce the water cement ratio of cement grout.
- Although the interfacial bond strength of C-SFPM was found to be improving with a decrease in the amount of water in the emulsified mixture at the time of grouting, the degree of variability associated with interfacial bond strength was found to be higher. Therefore, it is believed that more research work is needed in this direction to reduce the degree of variability associated with such evaluation.

ACKNOWLEDGEMENT

The work described in this paper was supported by a grant from the Research Grants Council of the Hong Kong Special Administrative Region, China (PolyU 15204022 for GRF project funded in 2022/23 Exercise) and partially supported by the National Science Fund for Young Scholars of China (No. 52208283).

.

AUTHOR CONTRIBUTIONS

The authors confirm contribution to the paper as follows: study conception and design: Zhen Leng, Prabin Kumar Ashish, Xing Cai; data collection: Prabin Kumar Ashish, Xing Cai, Zhifei Tan; analysis and interpretation of results: Xing Cai, Prabin Kumar Ashish; draft manuscript preparation: Xing Cai, Prabin Kumar Ashish; resources, funding acquisition, writing - review & editing: Zhen Leng, Hainian Wang, Prabin Kumar Ashish, Xing Cai. All authors reviewed the results and approved the final version of the manuscript.

REFERENCES

1. Oliveira, J. R. M. D. Grouted macadam: material characterisation for pavement design. Doctoral dissertation submitted to University of Nottingham, UK, 2017.
2. Oliveira, J. R., Thom, N. H., Zoorob, S. E.. Design of pavements incorporating grouted macadams. *Journal of Transportation Engineering*, 2008. 134(1), 7-14.
3. Corradini, A., Cerni, G., D'Alessandro, A., Ubertini, F. Improved understanding of grouted mixture fatigue behavior under indirect tensile test configuration. *Construction and Building Materials*, 2017. 155, 910-918.
4. Khan, M. I., Huat, H. Y., Dun, M. H. B. M., Sutanto, M. H., Jarghouyeh, E. N., Zoorob, S. E. Effect of irradiated and non-irradiated waste PET based cementitious grouts on flexural strength of semi-flexible pavement. *Materials*, 2019. https://doi.org/10.3390/ma12244133
5. Cai, X., Yang, J., Chen, X., Zhang, J., Zhang, H.. Interlocking property evaluation of dual skeleton in semi-flexible pavement material by micromechanical model and X-ray computed tomography. *Construction and Building Materials*, 2020a. https://doi.org/10.1016/j.conbuildmat.2020.118934

6. Cai, X., Zhang, J., Zhang, H., Yao, Z., Chen, X., Yang, J., 2020b. Identification of microstructural characteristics in semi-flexible pavement material using micromechanics and nano-techniques. Construction and Building Materials, 246, 118426. https://doi.org/10.1016/j.conbuildmat.2020.118426
7. Chen, X., Wang, Y., Chong, H., Huang, J., 2020. Use of Sulphoaluminate Cement in Grouted Macadam as Sustainable Pavement Material. Journal of Transportation Engineering, Part B: Pavements, 146(2), 04020018. https://doi.org/10.1061/JPEODX.0000167
8. Zapata, P., Gambatese, J. A.. Energy consumption of asphalt and reinforced concrete pavement materials and construction. *Journal of infrastructure systems*, 2005. 11(1), 9-20.
9. Frazer, L. Built environment: new default for asphalt?.2008. https://ehp.niehs.nih.gov/doi/10.1289/ehp.116-a379a (accessed on Jan.24, 2022).
10. Capitão, S. D., Picado-Santos, L. G., Martinho, F. Pavement engineering materials: Review on the use of warm-mix asphalt. *Construction and Building Materials*, 2012. 36, 1016-1024.
11. Rengarasu, T. M., Juzaafi, M., Bandara, W. M., Jegatheesan, N. Suitability of coal bottom ash and carbonized rice husk in hot mix asphalt. *Asian Transport Studies*, 2020. 6, 100013.
12. Jarrett, P. M., Beaty, A. N. S., Wojcik, A. S. Cold-mix asphalt technology at temperatures below 10 C (with discussion). *Association of Asphalt Paving Technologists Proceedings*, 1984. 53, 50-97.
13. Brown, S., Needham, D. A study of cement modified bitumen emulsion mixtures. *Association of Asphalt Paving Technologists (AAPT)*, 2000. 69, 92-121.
14. Chehovits, J., Galehouse, L. Energy usage and greenhouse gas emissions of pavement preservation processes for asphalt concrete pavements. Proceedings of the 1st International Conference of Pavement Preservation, 2010. 27-42.
15. Jain, S., Singh, B., 2021. Cold mix asphalt: An overview. *Journal of Cleaner Production*, 2021. https://doi.org/10.1016/j.jclepro.2020.124378
16. COP26: Together for our planet, UN Climate change conference 2021 (https://www.un.org/en/climatechange/cop26; accessed on Jan.11, 2022)
17. Al-Busaltan, S., Al Nageim, H., Atherton, W., Sharples, G., 2012. Mechanical properties of an upgrading cold-mix asphalt using waste materials. *Journal of materials in civil engineering, 24(12)*, 2012. 1484-1491.
18. Doyle, T. A., McNally, C., Gibney, A., Tabaković, A. Developing maturity methods for the assessment of cold-mix bituminous materials. *Construction and building materials*, 2013. 38, 524-529.
19. Ferrotti, G., Pasquini, E., Canestrari, F. Experimental characterization of high-performance fiber-reinforced cold mix asphalt mixtures. *Construction and Building Materials*, 2014. 57, 117-125.
20. Nassar, A. I., Mohammed, M. K., Thom, N., Parry, T. Mechanical, durability and

microstructure properties of Cold Asphalt Emulsion Mixtures with different types of filler. *Construction and Building Materials*, 2016. 114, 352-363.
21. Li, R., Leng, Z., Wang, Y., Zou, F. Characterization and correlation analysis of mechanical properties and electrical resistance of asphalt emulsion cold-mix asphalt. *Construction and Building Materials*, 2020. https://doi.org/10.1016/j.conbuildmat.2020.119974
22. Du, S. Mechanical properties and shrinkage characteristics of cement stabilized macadam with asphalt emulsion. *Construction and Building Materials*, 2019. 203, 408-416.
23. Tan, Y., Ouyang, J., Lv, J., Li, Y., 2013. Effect of emulsifier on cement hydration in cement asphalt mortar. *Construction and building Materials*, 2013. 47, 159-164.
24. Li, W., Hong, J., Zhu, X., Yang, D., Bai, Y., Liu, J., Miao, C. Retardation mechanism of anionic asphalt emulsion on the hydration of Portland cement. *Construction and Building Materials*, 2018. 163, 714-723.
25. Huo, J., Wang, Z., Zhang, T., He, R., Chen, H. Influences of interaction between cement and ionic paraffin emulsion on cement hydration. *Construction and Building Materials*, 2021. https://doi.org/10.1016/j.conbuildmat.2021.123951
26. Bharath, G., Shukla, M., Nagabushana, M. N., Chandra, S., Shaw, A. Laboratory and field evaluation of cement grouted bituminous mixes. *Road Materials and Pavement Design*, 2020. 21(6), 1694-1712.
27. Zachariah, J. P., Sarkar, P. P., Nandi, D. A study on the properties of cement grouted open-graded bituminous concrete with brick as aggregates. *Construction and Building Materials*, 2020. https://doi.org/10.1016/j.conbuildmat.2020.119436
28. Shukla, M., Gottumukkala, B., Nagabhushana, M. N., Chandra, S., Shaw, A., Das, S. Design and evaluation of mechanical properties of cement grouted bituminous mixes (CGBM). *Construction and Building Materials*, 2021. https://doi.org/10.1016/j.conbuildmat.2020.121805
29. Gupta, L., Kumar, R.Recarpeting using cement grouted bituminous mix in urban flexible pavement: a laboratory and field evaluation. *Australian Journal of Civil Engineering*, 2021. 19(2), 235-246.
30. Hassan, K., Setyawan, A., Zoorob, S. E. Effect of Cementitious Grouts on the Properties of Semi-Flexible Bituminous Pavements. *Proceedings of the 4th European Symposium on Performance of Bituminous and Hydraulic Materials in Pavements*, Nottingham, UK. 2002.
31. Mukherjee, D., Sahoo, U. C. Laboratory characterization of a cement grouted bituminous macadam made with Portland slag cement. *International Journal of Pavement Research and Technology*, 2019. 12(6), 574-580.
32. Al-Qadi, I. L., Gouru, H., Weyers, R. E., 1994. Asphalt Portland cement concrete composite: laboratory evaluation. *Journal of transportation engineering*, 1994. 120(1), 94-108.
33. Luo, S., Yang, X., Zhong, K., Yin, J. Open-graded asphalt concrete grouted by latex

modified cement mortar. *Road Materials and Pavement Design*, 2020. 21(1), 61-77.
34. Zarei, S., Ouyang, J., Yang, W., Zhao, Y., 2020. Experimental analysis of semi-flexible pavement by using an appropriate cement asphalt emulsion paste. *Construction and Building Materials*, 2020. https://doi.org/10.1016/j.conbuildmat.2019.116994
35. Kaushik, S., Siddagangaiah, A. K.. Characterisation of cement grouted bituminous mixes using marginal aggregates. *Road Materials and Pavement Design*, 2020. 1-18.
36. Fang, B., Xu, T., Shi, S. Laboratory study on cement slurry formulation and its strength mechanism for semi-flexible pavement. *Journal of Testing and Evaluation*, 2016. 44(2), 907-913.
37. Hou, S., Xu, T., Huang, K. Investigation into engineering properties and strength mechanism of grouted macadam composite materials. *International Journal of Pavement Engineering*, 2016. 17(10), 878-886.
38. Pei, J., Cai, J., Zou, D., Zhang, J., Li, R., Chen, X., Jin, L.. Design and performance validation of high-performance cement paste as a grouting material for semi-flexible pavement. *Construction and Building Materials*, 2016. 126, 206-217.
39. Hou, S., Xu, T., Huang, K. Aggregate gradation influence on grouting results and mix design of asphalt mixture skeleton for semi-flexible pavement. *Journal of Testing and Evaluation*, 2017. 45(2), 591-600.
40. Fang, Y., Wang, X., Jia, L., Liu, C., Zhao, Z., Chen, C., Zhang, Y.. Synergistic effect of polycarboxylate superplasticizer and silica fume on early properties of early high strength grouting material for semi-flexible pavement. *Construction and Building Materials*, 2022. https://doi.org/10.1016/j.conbuildmat.2021.126065
41. IRC:111.. Specifications for dense graded bituminous mixes. *Indian Road Congress*, New Delhi, India. 2009.
42. Ling, S., Hu, M., Sun, D., Ni, H., Xu, L. Mechanical properties of pouring semi-flexible pavement material and engineering estimation on contribution of each phase. *Construction and Building Materials*, 2022. https://doi.org/10.1016/j.conbuildmat.2021.125782
43. Marín-Uribe, C. R., Restrepo-Tamayo, L. M. Experimental study of the tensile strength of hot asphalt mixtures measured with indirect tensile and semi-circular bending tests. *Construction and Building Materials*, 2022. . https://doi.org/10.1016/j.conbuildmat.2022.127651
44. Zhong, K., Sun, M., Zhang, M., Qin, Y., Li, Y.. Interfacial and mechanical performance of grouted open-graded asphalt concrete with latex modified cement mortar. *Construction and Building Materials*, 2020. . https://doi.org/10.1016/j.conbuildmat.2019.117394
45. Paglia, C. S., Wombacher, F. J., Böhni, H. K. Hydration, strength, and microstructural development of high early-strength C(4)A(3)S activated burnt oil shale-based cement system. *ACI Materials Journal*, 2001. 98(5), 379-385.
46. Jiang, X., Zhu, H., Yan, Z., Zhang, F., Ye, F., Li, P., Zhang, X., Dai, Z., Bai, Y., & Huang, B.. A state-of-art review on development and progress of backfill grouting

materials for shield tunneling. *Developments in the Built Environment*, 2023, 100250. https://doi.org/10.1016/j.dibe.2023.100250

47. Moffatt, E. G., Thomas, M. D. Durability of rapid-strength concrete produced with ettringite-based binders. *ACI Materials Journal*, 2018. 115(1), 105-115.

Yu, J., Qian, J., Tang, J., Ji, Z., Fan, Y. Effect of ettringite seed crystals on the properties of calcium sulphoaluminate cement. *Construction and Building Materials*, 2019. 207, 249-257.